NJC

Accepted Manuscript

This is an *Accepted Manuscript*, which has been through the Royal Society of Chemistry peer review process and has been accepted for publication.

Accepted Manuscripts are published online shortly after acceptance, before technical editing, formatting and proof reading. Using this free service, authors can make their results available to the community, in citable form, before we publish the edited article. We will replace this *Accepted Manuscript* with the edited and formatted *Advance Article* as soon as it is available.

You can find more information about *Accepted Manuscripts* in the Information for Authors.

Please note that technical editing may introduce minor changes to the text and/or graphics, which may alter content. The journal's standard Terms & Conditions and the Ethical guidelines still apply. In no event shall the Royal Society of Chemistry be held responsible for any errors or omissions in this *Accepted Manuscript* or any consequences arising from the use of any information it contains.

ROYAL SOCIETY OF CHEMISTRY

www.rsc.org/njc

Journal Name

ARTICLE

Structure, formation, thermodynamics and interactions in 9-carboxy-10-methylacridinium-based molecular systems†

Received 00th January 20xx,
Accepted 00th January 20xx

DOI: 10.1039/x0xx00000x

www.rsc.org/

Damian Trzybiński,[a] Beata Zadykowicz,[b] Michał Wera,[b] Illia E. Serdiuk,[b] Andrzej Sieradzan,[b,c] Artur Sikorski,[b] Piotr Storoniak[b] and Karol Krzymiński[b*]

9-Carboxy-10-methylacridinium chloride and trifluoromethanesulfonate, the parent compounds for a wide sort of chemiluminogenic salts of practical importance, were synthesized and thoroughly investigated to address problems concerning structural and thermodynamical issues of those cognitively interesting molecular systems. At various conditions of crystallization, the title salts disclosed three types of crystals – one built of the monomeric form of cations and the two containing homoconjugated cations. The title compounds make the first described derivatives of acridine, expressing homoconjugated cationic forms – both in crystalline solid and gaseous phases. The monocrystals were widely characterized, employing X-ray crystallography and spectroscopic methods such as MALDI-TOF MS, NMR and UV-VIS. X-ray crystallography studies revealed the occurrence of the three completely different molecular architectures, in which not only the counter ions and stoichiometry, but also the space group and number of molecules in the unit cell are different. The energetics and intermolecular interactions occuring within the crystals were explored applying crystal lattice energy calculations and Hirshfeld surface analysis. In order to elucidate the thermodynamics and origin of experimentally revealed forms, the computations basing on the Density Functional Theory were performed, assuming vapour and liquid phases.

Introduction

Derivatives of acridine-9-carboxylic acid (ACA) are widely investigated and applied group of compounds due to their ability for effective luminescence in aqueous or organic environments[1–4] as well as they exhibit an interesting physicochemical properties.[5–7] ACA, the parent molecule in this family of compounds, makes a simple heteroaromatic system, differing from its hydrocarbon analogue, anthracene-9-carboxylic acid, in terms of presence an electron-attracting nitrogen atom in the central aromatic ring at the *para* position to the carboxyl group. The endocyclic N atom present in ACA causes slight change in π-electronic energy levels as compared to those in anthracene-9-carboxylic acid and diminution of charge transfer from the aromatic ring system to the carboxyl fragment.[5] Theoretical studies carried on the ACA molecule indicated that, in the ground state, the carboxyl group is oriented at an angle of about 55° relative to the plane of the acridine moiety, while in the excited state (S_1) the –COOH fragment twists, which is accompanied by the flattening of the molecular arrangement.[5] In aqueous liquid phase, ACA – in addition to its neutral form – may appear as zwitterions or monocations, depending on the acidity of environment.[5]

The compounds under study, containing N-methylated ACA moiety, are the simplest and oldest acridinium derivatives investigated in the context of chemiluminescence phenomenon.[8] 9-Carboxy-10-methylacridinium cations (CMA) make the structural base of a wide sort of chemiluminogenic compounds, that have been widely employed as labels and indicators – a specially designed molecular systems utilized in medical diagnostics and trace analysis.[9] However, derivatives of CMA are also interesting from the cognitive point of view. CMA, similarly to ACA and related molecular systems, can

[a] *Faculty of Chemistry, Biological and Chemical Research Centre, University of Warsaw, Żwirki i Wigury 101, 02-089 Warsaw, Poland.*
[b] *Faculty of Chemistry, University of Gdańsk, Wita Stwosza 63, 80–308 Gdańsk, Poland. E-mail: karol.krzyminski@ug.edu.pl*
[c] *Blirt S.A., Trzy Lipy 3/1.38, 80-172 Gdańsk, Poland.*

† Electronic Supplementary Information (ESI) available: synthesis, chemical data and canonical structures of the investigated crystals (**1**–**3**) (Scheme S1†, Scheme S2†) and their precursors (Fig. S15†), crystal data and structure refinement for **1**–**3** (Table S5†), parameters of hydrogen bondings found in **1**–**3** (Tables S6†, S8†, S11†), parameters of π–π interactions (Tables S7†, S9†, S12†), parameters of Cl···O contacts (Table S10†), crystal packing in **1**–**3** (Figs S4†, S5†, S6†), CSD database data (Figs S7†, S8†), chemical shifts of **1**–**3** in ^{1}H and ^{13}C NMR spectra (Table S1†), MALDI-TOF MS data (Tables S2†–S3†, Fig. S2†), the Hirshfeld surfaces representing distances external and internal to the surface for **1**–**3** (Fig. S9†) and fingerprint plots of acridinium moieties in **1**–**3**, spectrophotometric titration data for **1** (Fig. S14†, Table S4†) Structural parameters of **1**–**3** (Tab. S13†) and thermodynamic data for monomeric and dimeric conformers of **1** and **2**. Crystallographic structure data based on the single-crystal diffraction has been deposited in the Cambridge Crystallographic Data Center (CCDC 981470, CCDC 981472 and CCDC 981471). These data can be obtained free of charge at www.ccdc.cam.ac.uk/conts/retrieving.html [or from the Cambridge Crystallographic Data Centre (CCDC), 12 Union Road, Cambridge CB2 1EZ, UK; fax: + 44(0)1223-336033; email: deposit@ccdc. cam.ac.uk]. See DOI: 10.1039/x0xx00000x

occur in liquid phases in various forms, depending on the degree of their ionization.[10] Structural similarity of CMA to betaines and isonicotinic acids is an intriguing fact in the context, that the latter compounds are able to interact effectively with biological molecules through the formation of complexes or by a wide range of short-range interactions.[11] As other carboxylic acids, molecules of CMA are prone to formation of H-bonded forms, involving a carboxyl group, which opens up an opportunities for them to occur in various structural forms.

The molecular architecture and the intermolecular interactions, occurring in various phases in the group of quaternary salts, containing 9-carboxy-10-methylacridinium or hydrogen bis(9-carboxy-10-methylacridinium) cations and chloride or trifluoromethanesulfonate (triflate) anions, were the main tasks of presented work. The above mentioned molecular systems, adopting various crystalline forms – denoted as **1**, **2** and **3** – contain structural moieties, that have been implemented in the originating from CMA chemiluminogenic salts of practical importance.[1,9] We were primarily focused on the investigation of various crystalline forms with the participation of CMA – as we were interested of how many structural variants and at what conditions they may appear in solid, gaseous and liquid phases. We assumed that an extensive analysis of the structural problems concerning CMA-based cationic forms may be helpful to disclose the factors determining chemical and physicochemical properties of a wide sort of relative acridinium salts. As CMA makes one of the products secreted upon chemiluminescence of acridinium esters and sulphonamides, the structural study presented here may also shed some light on the course of this complicated process, that have been studied by us for a long time.[2,12,13] In this work we employed a broad set of experimental methods such as single crystal X-ray crystallography and spectroscopic techniques, including UV-VIS, ^{1}H and ^{13}C NMR and MALDI-TOF mass spectrometry. Moreover, we also applied various theoretical tools, such as determination of Hirshfeld surfaces, calculation of crystal lattice energies as well as computations at the level of Density Functional Theory (DFT). All these approaches brought us a chance to take a deep look at the intermolecular interactions occurring among a neighboring fragments of molecules and cations in various forms, energetics of cohesion forces in crystals and the "molecular shapes", characteristic for crystalline solid phases. Quantum chemistry calculations disclosed information concerning structural and thermodynamic aspects of the investigated compounds, their stabilities in gaseous and liquid phases and enabled us to propose a pathways, leading to the formation of CMA-based molecular systems described here.

Experimental

Single crystal X-ray diffraction analysis and refinement

Two acridinium salts, namely 9-carboxy-10-methylacridinium chloride (CMACl) and 9-carboxy-10-methylacridinium trifluoromethanesulfonate (CMATfO), were prepared and analysed for chemical identity, as it is given Electronic Supplementary Information†. The latter compounds were subjected to crystallization at various conditions. According to that, CMACl was dissolved in DI water (UP class), acidified with HCl and the solution was heated up to boiling, than cooled to 298 K and left over molecular sieves until gradual evaporation of the solvents. This way the crystals of the compound **1**, namely 9-carboxy-10-methylacridinium chloride dihydrate, were grown. Additionally, CMACl was dissolved in an ethanol/water phase (1/9 *v*/*v*) and left at 298 K to enable growth of crystals of the compound **2**, namely hydrogen bis(9-carboxy-10-methylacridinium) chloride dihydrate, sufficient for X-ray diffraction studies. Similarly, CMATfO was dissolved in ethanol/water mixture (1/9 *v*/*v*), filtered and left aside at r.t. to obtain good quality crystals of hydrogen bis(9-carboxy-10-methylacridinium) trifluoromethanesulfonate (**3**).

Diffraction measurements were performed using *Oxford Diffraction Gemini R ULTRA Ruby CCD* diffractometer with Mo*K*α (λ = 0.71073 Å) radiation. Data collection and cell refinement were carried out with *CrysAlis CCD* and data reduction with *CrysAlis RED* software[14] applying multiscan absorption corrections (empirical absorption correction basing on spherical harmonics, implemented in *SCALE3 ABSPACK* scaling algorithm). The *SHELXS-97* package was used to solve the structures by direct methods and *SHELXL-97* to carry out refinements by full-matrix least-squares on F^2.[15] The H-atoms bound to carboxylic oxygen atoms in **2** and **3** were located in a Fourier-difference map and refined freely with occupancy factors of 0.5. The H-atom bound to carboxylic oxygen atom in **1** was located in a Fourier difference map and refined as riding with U_{iso}(H) = 1.5U_{eq}(O). In all cases the water H atoms were located in a Fourier-difference map, restrained by DFIX command 0.85 for O–H distances and by DFIX 1.39 for H···H distance and refined as riding with $\mathbf{U}_{iso}$(H) = 1.5U_{eq}(O). All other H-atoms were positioned geometrically, with C–H = 0.93 Å and 0.96 Å for the aromatic and methyl H-atoms, respectively, and constrained to ride on their parent atoms with U_{iso}(H) = xU_{eq}(C), where x = 1.2 for the aromatic H-atoms and x = 1.5 for the methyl H-atoms. All interactions demonstrated were found by *PLATON* program.[16] To prepare molecular graphics, *ORTEPII*,[17] *PLUTO-78*[18] and *Mercury*[19] programs were employed.

Crystal lattice energies

The lattice energies (E_L), reflecting the global energetics of interactions within crystals, were obtained using X-ray structures of investigated compounds **1**–**3**. We have performed calculations employing the General Utility Lattice Program (GULP, version 4.0), which is based on the force field methods approach.[20] The GULP computations allow for evaluation of the lattice energy as the sum of three components: the energy of the long-range Coulomb interactions (E_{el}) and energies of the dispersive (E_d) and repulsive (E_r) interactions (eq. 1):

$$E_L = E_{el} + E_d + E_r \quad (1)$$

The Coulomb energy was calculated according to the expression given by Coulomb's law. Relative atomic partial charges, necessary for prediction of E_{el} values, were obtained at the Density Functional Theory (DFT) level[21] by reproducing the electrostatic potential around molecules (ESP fit charges).[22] DFT single-point computations were conducted in the gas phase for aggregates of molecules preserving geometries and their relative arrangement as in the crystal phase. In these calculations the M06-2X functional[23] was employed together with the 6-31++G** basis set.[24] Calculations were carried out using the Gaussian 09 program.[25] Two-body short-range interactions, contributing as E_d and E_r terms to the lattice energy, were described by Buckingham potential available within GULP (eq. 2):

$$-C_6/R^6 + A\exp(-R/\rho) \quad (2)$$

In the above expression, C_6, A and ρ denote the atomic parameters for the pairs of interacting atoms and R represents the interatomic distances between atoms in the reference cell and atoms in the neighbouring cells. Potential parameters, describing interactions involving F atom were taken from Ref.[26], whereas parameters for the remaining atoms – from Ref.[27]

Such an approach was demonstrated to be successful in prediction of the sublimation energies for related acridinium derivatives.[7,28]

Hirshfeld surface analysis

The investigation of packing modes and intermolecular interactions in crystals was carried out using Hirshfeld surfaces to partition the crystal space. Hirshfeld surfaces and fingerprint plots facilitate the comparison of intermolecular interactions in building different supramolecular motifs in the crystal structure. Molecular geometries, taken directly from resolved crystal structures of **1**–**3**, were used for generating the Hirshfeld surfaces and two-dimensional fingerprint plots with the assistance of the *Crystal Explorer 3.1* program.[29] A complementary two-dimensional mappings are also presented, which summarize quantitatively the types of intermolecular contacts experienced by chemical entities in the bulk.

Spectroscopic and spectrometric measurements

^{1}H and ^{13}C NMR spectra for compounds **1**–**3** in deuterium oxide, dimethyl sulfoxide-d_6, acetonitrile-d_3 and methanol-d_4 were recorded at r.t. using *Varian Unity 500 Plus* spectrometer with 5 mm PFG probe attached. Additionally, molecular systems presenting various forms in solid crystalline phase (**1** and **2**), were subjected to ^{1}H NMR experiments in CD_3OD at standard (298 K) and lowered temperature (233 K). The signals of protons in ^{1}H NMR were attributed with the aid of ^{1}H–^{1}H COSY spectra and the carbon-13 signals were attributed with the assistance of ^{1}H–^{13}C HETCOR (ghmbc) spectra and ACD HNMR and CNMR software (*Cambridge*),[30] respectively. The NMR data is summarized in Table S1† and selected spectra are presented in Figs S1† and S2†.

The mass spectra of **1**–**3** were recorded employing *Biflex III* MALDI-TOF mass spectrometer, working in the positive polarity mode with the 150–600 m/z range of scan and the attenuation of the laser beam set at 60%. The samples of **1**–**3** (3–5 mg) were dissolved in the mixture consisting of dihydroxybenzoic acid (DHBA) and water. Additionally, samples of **1**–**3** were dehydrated (denoted as **1dh**, **2dh**, **3dh**) and dissolved in non-aqueous matrix (DHBA/anhydrous acetonitrile) and the above mixtures were also subjected to MALDI-TOF MS experiments. Results obtained for **1**, **2** and **3** and **1dh**, **2dh**, **3dh** are summarized in Tables S2† and S3† and exemplary mass spectra are presented in Fig. S2†.

The ionization constant (pK_a), denoting protolytic dissociation of the monocationic (c) to zwitterionic (z) form of **1** (K_a = [**1z**][H_3O^+]/[**1c**]) was obtained by spectrophotometric acid-base titration at 298 K in water-ethanol (9:1, *v*:*v*) solutions (Table S4†, Fig. S3†). To a stirred solution of **1** (2.00 ml, 2.50×10^{-5} M) in DI H_2O (UP-grade), concentrated hydrochloric acid was gradually added in 10–100 µl portions until the final volume of 4.00 ml was attained. The actual pH of the mixtures with c(HCl) < 0.1 M was assessed using portable pH-meter (*GPX-105s*, *Elmetron*, Poland). The acidity constants (H_0) were determined instead of pH for the highly acidic mixtures,[31,32] using mass concentration of HCl in the cell, established gravimetrically after each addition. The electronic absorption UV-Vis spectra for each solution were recorded using *Lambda 40* UV-Vis spectrophotometer (*Perkin-Elmer*, USA) in the range of 300–500 nm (slit = 1 nm). The registered spectra were multiplied by the dilution coefficient d ($d = V_i/V_0$, where V_i is volume of actual solution, in ml; V_0 is the volume of the starting solution, 2.00 ml). To calculate the values of pK_a by monitoring changes in absorbance at selected wavelengths, the Henderson-Hasselbalch equation, implemented in *Spectra Data Lab* software,[33] was applied. The latter method relates pH and pK_a to the equilibrium concentrations of dissociated [A^-] and non-dissociated form [HA] of the acid, according to the equation (eq. 3):[34]

$$pH = pK_a + \log([A^-]/[HA]) \quad (3)$$

The medium effects, associated with the high content of acid in concentrated HCl solutions, were corrected according to the Haldna method.[35]

Computations

Unconstrained geometry optimizations of isolated cations and their dimeric forms involved in **1**–**3** complexes with counter ions (Cl^-, $CF_3OSO_2^-$) and water molecules were carried out at the DFT level of theory[21] using gradient techniques[36] and the 6-31G** basis set.[37] The calculations were carried out with the B3LYP functional, in which Becke's nonlocal exchange[38] and the Lee-Yang-Parr correlation functionals[39] were applied. After completion of each optimization, the Hessian (second derivatives of the energy as a function of the nuclear coordinates) was calculated to assess whether stationary structures had been obtained.[21,37b] The harmonic vibrational frequencies were then derived from the numerical values of these second derivatives and used to obtain the Gibbs' free energy contributions at 298.15 K and standard pressure with the aid of a built-in computational program of statistical thermodynamics routines.[40] All quantum chemical calculations were performed with the Gaussian 09[25] program, while the

plots showing the molecular structures were generated with the aim of the *ChemCraft* program.[41]

Results and discussion

Crystal architecture riddles

9-Carboxy-10-methylacridinium chloride dihydrate (1)

Compound **1**, whose molecular structure is depicted in Fig. 1A, crystallizes in the monoclinic $P2_1/n$ space group with four ion pairs and eight water molecules in the unit cell (Table S5†). The bond lengths and angles, characterizing the geometry of the acridine moiety in **1**, are similar to other already reported salts.[42–48] The acridine ring system is almost planar (the average deviation from planarity is 0.0239(3) Å), while carboxyl group is twisted at an angle of 89.6(1)° relative to the acridine skeleton. The mean planes of adjacent acridinium moieties are either parallel or inclined at an angle of 25.5(1)° in the crystal lattice. The packing of ions and water molecules in **1** is affected by O–H···O, O–H···Cl and π-π stacking intermolecular interactions and contacts (Figs 1, 2 and S4†, Tables S6† and S7†, CCDC 981470). The carboxylic

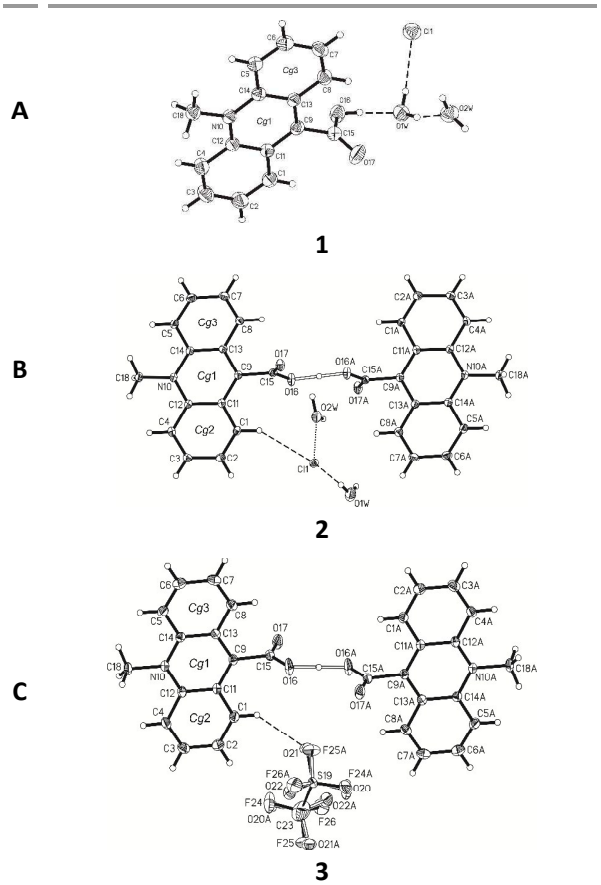

Fig. 1 The molecular structure of crystalline compound **1** (graph A), **2** (graph B) and **3** (graph C) showing the atom labeling scheme. Displacement ellipsoids are drawn at the 25% probability level and H-atoms are shown as small spheres of arbitrary radius. *Cg*1 and *Cg*2 and *Cg*3 denote the ring centroids. The O–H···O, O–H···Cl, O–H···Cl, C–H···Cl hydrogen bonds and O···Cl contacts are represented by dashed lines.

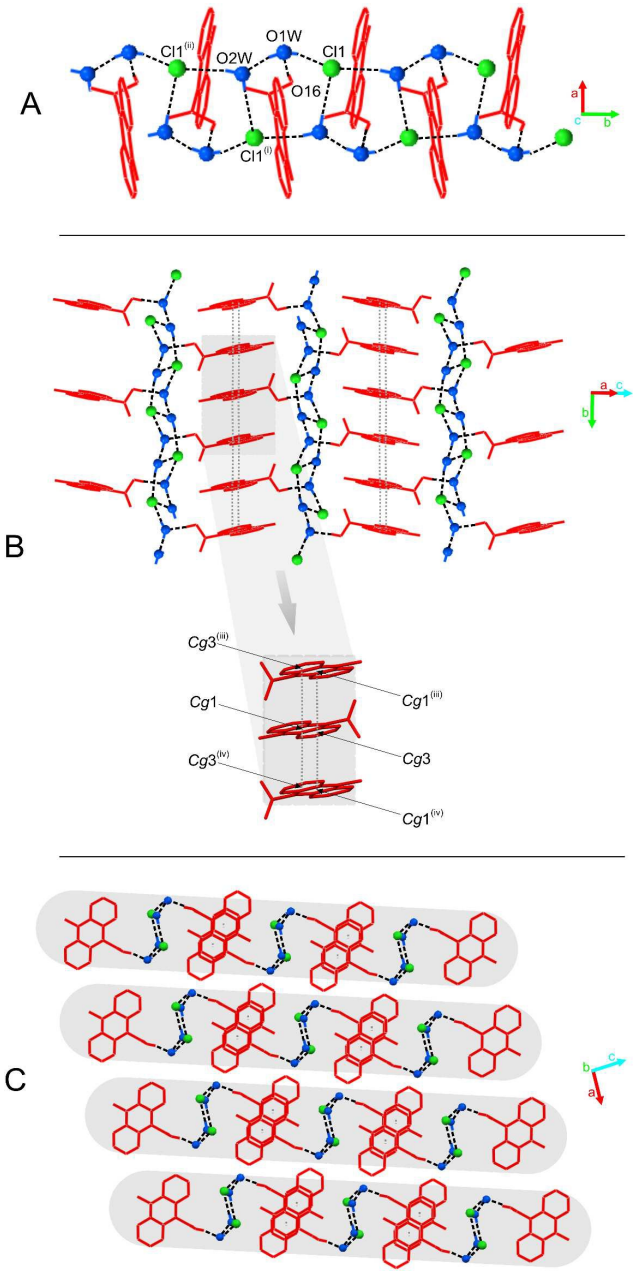

Fig. 2 The supramolecular architecture in the crystal of **1**: (**A**) the ladder-like chain running along [010] direction; (**B**) single layer stabilized by the π–π stacking interactions between aromatic rings of adjacent acridinium moieties; (**C**) the global framework of ions and water molecules in the crystal in parallel sheets. [Symmetry codes: (i) –x + 1/2, y – 1/2, –z + 3/2; (ii) x, y – 1, z; (iii) –x, –y, –z + 1; (iv) –x, –y + 1, –z +1].

hydrogen atom involved in each cation interacts with one water molecule through the O–H···O hydrogen bond (length 2.471(3) Å). Water molecule linked to the cation is further (H-bonded to another water molecule and chloride anion lengths 2.666(4) and 3.041(2) Å, respectively). Each water molecule, not directly H-bonded to cation, participates in O–H···Cl hydrogen bonds with two chloride anions (lengths 3.121(3) and 3.133(3) Å). The above described interactions infinitely repeated are disclosed in a ladder-like chain running along [010] direction (Fig. 2A). Three water molecules and two

chloride anions, participating in the above-mentioned chains, are arranged in characteristic five-membered rings of $R_5^3(10)$ motif. Inversely oriented parallel chains are tied together into the sheet, formed by the intermolecular π–π stacking interactions between adjacent acridinium moieties (Fig. 2B). The crystal lattice of 1 is further stabilized by non-specific dispersive interactions between inversely oriented parallel sheets (Fig. 2C).

Hydrogen bis(9-carboxy-10-methylacridinium) chloride dihydrate (2)

Compound **2**, whose molecular arrangement is demonstrated in Fig. 1B, crystallizes in the monoclinic $P2_1/n$ space group with two ion pairs and four water molecules in the unit cell (Table S5†). In homoconjugated cation of hydrogen bis(9-carboxy-10-methylacridinium) involved in this compound, symmetric O–H···O hydrogen bond occurs (length 2.435(3) Å), in which the H-atom is located directly in the inversion centre. The chloride anion is found in two special positions, related by an inversion centre, with site occupancy factors of 0.5. The bond lengths and angles, characterizing the geometry of the acridine moieties in the cation, are characteristic for acridinium salts.[42–48] The two acridine ring systems are almost planar (the average deviation from planarity is 0.0311(3) Å) and parallel 0.0(0)°. The carboxyl groups are twisted at an angle of 84.8(1)° in respect to the relevant acridine skeletons. Acridinium moieties of adjacent cations are either parallel (remain at an angle of 0.0(1)°) or inclined at an angle of 23.6(1)°. Predominant role in packing of ions and water molecules in the crystals of **2** play O–H···Cl, C–H···O, C–H···Cl, π–π and Cl···O intermolecular interactions and contacts (Figs 1, 3 and S5†, Tables S8†–S10†, CCDC 981472). Each homoconjugated cation links two chloride anions *via* C–H···Cl interactions (lengths 3.560(3) and 3.735(3) Å). In turn, each chloride anion interacts with two water molecules by O–H···Cl hydrogen bonds (lengths 2.904(2) and 2.937(3) Å) and with one water molecule *via* O···Cl contact. Water molecules interact with neighbouring water molecules *via* O–H···O hydrogen bonds (length 2.820(4) Å), while cations interact by O–H···O (carbonyl) (length 3.117(4) Å) and C–H···O (length 3.519 Å) bonds. Repetition of some of the above described O–H···O, O–H···Cl and C–H···Cl interactions brings about formation of infinite chain of ions and water molecules running along [010] direction (Fig. 3A). Parallely oriented chains are tied by π–π stacking interactions between aromatic rings of adjacent acridinium moieties (Fig. 3B) and C–H···Cl hydrogen bonds between the H-atoms of methyl groups of cations and chloride anions into sheet spread out in [110] plane. Alternately oriented sheets constitute the crystal lattice of **2**, which is stabilized by the network of Cl···O contacts between chloride anions and water molecules as well as C–H···O interactions involving H-atoms of the acridinium fragments and water molecules (Fig. 3C).

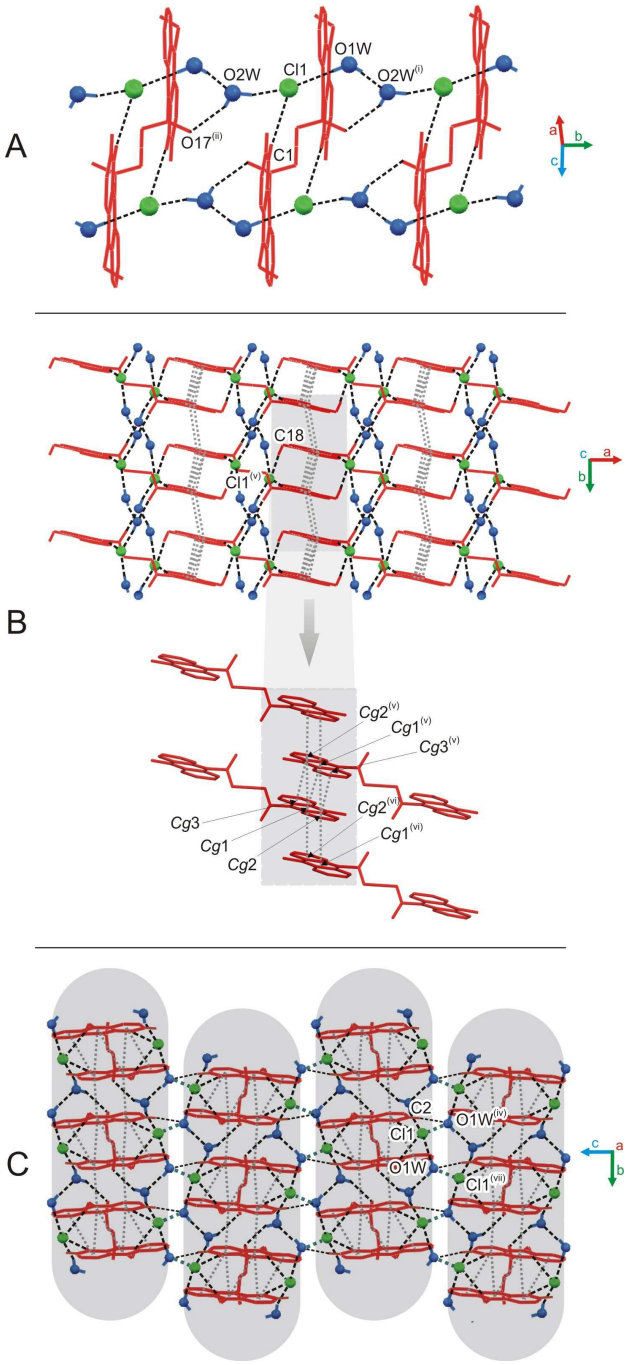

Fig. 3 The supramolecular architecture in the crystal of **2**: (**A**) complex chain built of ions and crystal water molecules running along [010] direction; (**B**) single layer stabilized by the π-π stacking interactions between rings of neighboring acridinium moieties spread out in [110] plane; (**C**) inversely oriented sheets linked by the network of O···Cl contacts between chloride anions and water molecules [Symmetry codes: (i) x, y + 1, z; (ii) –x + 2, –y, –z + 1; (iv) –x + 1, –y + 1, –z + 1; (v) –x + 1, –y, –z + 1; (vi) –x + 3/2, y – 1/2, –z + 1/2].

Hydrogen bis(9-carboxy-10-methylacridinium) trifluoromethane-sulfonate (3)

Compound **3**, whose molecular structure is demonstrated in Fig. 1C, crystallizes in the triclinic *P*-1 space group with one ion pair in the unit cell (Table S5†). In homoconjugated hydrogen bis(9-carboxy-10-methylacridinium) cation found in this compound, similarly to some other acid salts of carboxylic

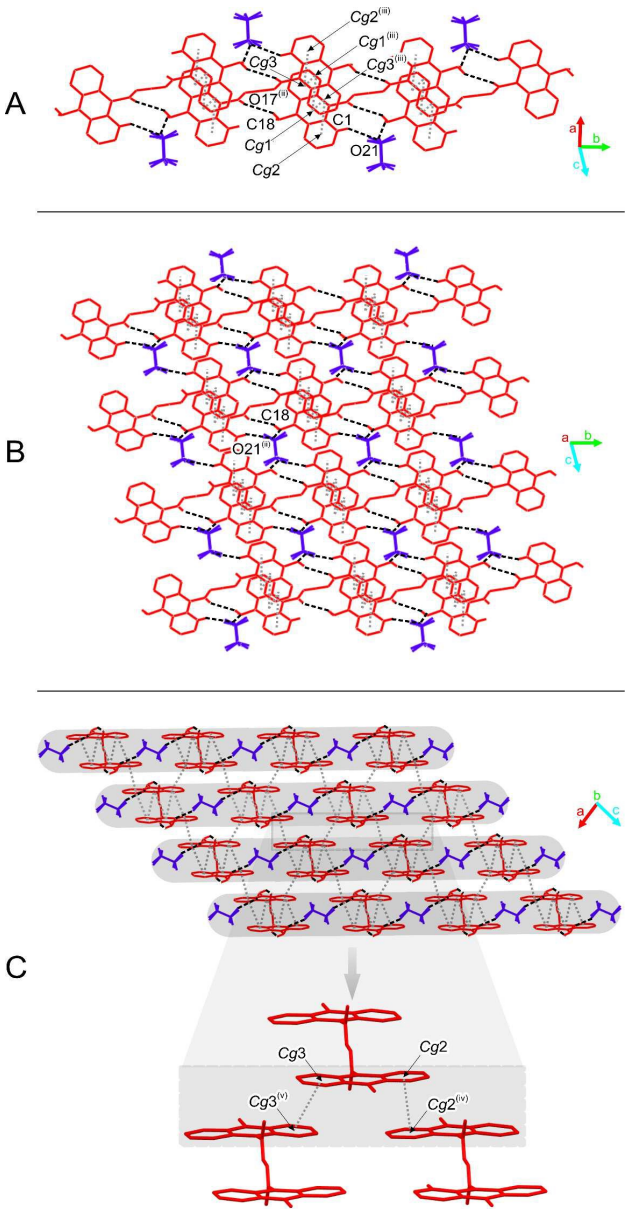

Fig. 4 Supramolecular architecture in the crystal of **3**: (**A**) infinite chain built of homoconjugated cations and anions running along [010] direction; (**B**) single layer of ions spread out in [101] plane; (**C**) multilayered framework of ions [Symmetry codes: (ii) x, y – 1, z; (iii) –x + 2, –y + 1, –z; (iv) –x + 2, –y + 1, –z + 1; (v) –x + 3, –y + 1, –z].

acids,[49–52] symmetric O–H···O hydrogen bonds occurs, in which the H-atom is located directly in the inversion centre (length 2.449(2) Å). The triflate anions ($CF_3OSO_2^-$) occupy two positions, with occupancy factor of 0.5 for S19, O21–22, C23, F24–26 and S19A, O21A–O22A, C23A, F24A–F26A, related to the inversion centre. The bond lengths and angles, characterizing the geometry of the acridinium moieties in the cation, are similar to other acridinium-based derivatives.[42–45] Two acridine ring systems in the cation are almost planar (the average deviation from planarity is 0.0505(3) Å and parallel 0.0(0)°. The carboxyl groups are twisted at an angle of 84.2(1)° relative to the relevant acridine skeleton. Acridinium moieties of adjacent cations are parallel in the crystal lattice, remaining at an angle of 0.0(1)°.

Predominant role in the packing of ions in the crystal of **3** play C–H···O and π–π intermolecular interactions (Figs 1, 4 and S6†, Tables S11† and S12†, CCDC 981471). Each homoconjugated cation interacts with neighbouring cation and anion through weak C–H···O hydrogen bonds involving methyl H-atom and carbonyl oxygen atom (length 3.199 Å) or methyl or acridine skeleton H atoms and O atom of triflate anion (lengths 3.360(20) and 3.370(30) Å, respectively).

Repetition of some of the above mentioned C–H···O interactions brings about formation of endless chain of ions running along [001] direction (Fig. 4A). Parallely oriented chains are linked by the network of C–H···O (involving methyl H atoms and O atoms of anions) and π–π intermolecular interactions (between aromatic rings of neighbouring acridinium moieties) forming layers spreading along (011) plane (Fig. 4B). Parallely oriented layers are stabilized by the network of π–π intermolecular interactions between aromatic rings of adjacent acridinium moieties, which results in the formation of continuous multi-layered framework of ions in the crystal (Fig. 4C).

Cambridge Structural Database analysis of O–H···O hydrogen bond

To have an insight how geometric parameters of O···H···O hydrogen bonds occurring in homoconjugated hydrogen bis(9-carboxy-10-methylacridinium) cations involved in compounds **2** and **3** relate to those in other compounds containing ions of such type, we carried out search in the *Cambridge Structural Database* (version 5.32) using program *CONQUEST*. The geometrical query with the following limiting criteria: no polymeric, no errors, no powder structures and only organics with 3D coordinates determined is depicted in Fig. S7†. Between 25 structures disclosed, 23 possess the hydrogen atom placed strictly in the middle of the O···H···O interaction (DIST1 = DIST2). Among the homoconjugated cations found, only 3 represented nitrogen-containing heteroaromatic systems.

The scaterrograms correlating lengths of hydrogen bonds (DIST1 and DIST2) and histogram imaging the distribution of the O···O distances (DIST3) in homoconjugated cations of 23 aromatic carboxylic systems are demonstrated in Fig. S8†. Analysis of the data stored in the *Cambridge Structural Database* and summarized in the latter figures discloses that the length of symmetrical O···H···O hydrogen bonds spans from 1.21 to 1.24 Å and O···O distances from 2.422 to 2.480 Å. Values of the length of hydrogen bonds and O···O distances in **2** and **3**, that equal to 1.22, 1.22 and 2.435(3), 2.449(2) Å, respectively – well comprise between the above invoked values.

Global and local interactions characterizing the crystal lattices

Energetics of the crystal lattices

An important thermodynamic characteristic of crystalline compounds is the crystal lattice energy, E_L, which reflects the strength of cohesion forces occurring within this kind of solid phase. Theoretical cohesive energies may be compared with the lattice energies, assessed on the base of experimental data (enthalpies of sublimation). In the past, employing the same computational methodology as in the current study, we

predicted E_L for a series phenyl acridine-9-carboxylates and satisfactory correlations with the experimental data were found.[7] The theoretical lattice energies were also obtained for several 9-phenoxycarbonyl-10-methylacridinium triflates, containing CMA as a structural fragment.[7] However, for the latter compounds – similarly as in the case of compounds **1**, **2** and **3** – experimental thermodynamic characteristics were not available. In such cases computer-aided simulations appear to be the only strategy to gain information regarding thermodynamic properties of investigated crystals. The E_L values characterizing **1**–**3**, calculated together with the electrostatic (E_{el}), dispersive (E_d) and repulsive (E_r) contributions to E_L are summarized in Table 1.

Predicted high values of E_L reflect substantial ionic character of lattices investigated herein (for comparison, purely molecular crystals of phenyl acridine-9-carboxylate derivatives studied previously were characterized by E_L of the magnitude around –160 kJ mol^{-1})[7].

The strongest cohesion force was found for **3** (E_L equals –653 kJ mol^{-1}). Lattice of compound **1** is less stable than the lattice of **3** by ca. 80 kJ mol^{-1} (E_L equals –575 kJ mol^{-1}), whereas the lattice of **2** is less stable by almost 120 kJ mol^{-1} when compared to **3** (E_L equals to –535 kJ mol^{-1}).

Various thermodynamic stabilities of investigated compounds result from different contributions of E_{el}, E_d and E_r to their total lattice energy. For **1** we have predicted the largest Coulomb term E_{el} among investigated crystals, which constitutes dominating contribution to E_L of this compound (–548 kJ mol^{-1}). Values of E_{el}, obtained for crystals containing the homoconjugated forms of cations, are smaller by about 240 kJ mol^{-1} (**2**) and 150 kJ mol^{-1} (**3**).

Compound **2** – which appears to be the least stable among investigated crystals – distinguishes from the others because of the high value of the dispersion term (–472 kJ mol^{-1}), which surpasses its electrostatic term (–312 kJ mol^{-1}). In contrast, dispersive attractions, represented by E_d term, in the case of **1** and **3** are smaller than the coulombic forces. It may also be noted that E_d term in **3** assumes similar value to E_{el} calculated for this compound (–398 *vs.* –356 kJ mol^{-1}) and both terms significantly overcome repulsive forces within the crystal lattice (E_r = 101 kJ mol^{-1}). As regards repulsion, compounds involving chloride anions and water molecules (**1**, **2**) exhibit almost identical E_r term, ca. 250 kJ mol^{-1}.

Table 1 Theoretical lattice energies (E_L) calculated using GULP and contributions to the lattice energies: E_{el} (Coulomb energy), E_d and E_r (dispersion and repulsion energy, respectively, calculated according to Buckingham's potential). All values are in kJ mol^{-1}.

Compound no.	E_{el}	E_d	E_r	$E_L = E_{el} + E_d + E_r$
1	−548.5	−281.3	254.9	−575.0
	−358.1 [a]	−150.7 [a]	48.2 [a]	−460.5 [a]
2	−312.3	−471.7	248.6	−535.4
	−240.0 [a]	−290.5 [a]	98.6 [a]	−432.0 [a]
3	−398.1	−355.6	100.6	−653.1

[a] Values calculated for lattices neglecting the presence of water molecules

To estimate the influence of water molecules on the cohesive forces occurring within the crystalline solid phases of **1** and **2**, we performed additional calculations involving crystals, from which we removed the water. Resulting E_L values along with the corresponding contributions (labelled with superscript a) are shown in Table 1.

When comparing the E_L and E_L^a values collected in Table 1, it can be observed that neglecting of water molecules leads to the destabilization of crystals **1** and **2** by 115 and 103 kJ mol^{-1}, respectively. Despite similar decrease of the total cohesive forces within **1** and **2** upon removing of water, the changes of individual components of E_L are not uniform. Thus, reducing of E_{el} in **1** amounts to 190 kJ mol^{-1}, while in **2** – to 72 kJ mol^{-1} (Table 1). In turn, the larger decrease of E_d takes place in **2** than in **1** (180 *vs.* 131 kJ mol^{-1}). Taking into account the sum of the E_{el} and E_d values, it can be estimated that co-crystallized water molecules introduce an attractive interactions into the crystal lattices equal to –321 kJ mol^{-1} (**1**) and –253 kJ mol^{-1} (**2**). Moreover, water molecules exert also significant repulsive effect, which in the case of **1** amounts to 207 kJ mol^{-1} and in case of **2** – 150 kJ mol^{-1}. Interestingly, removing of water from **2** yields the E_r value (98.6 kJ mol^{-1}), being almost identical as that predicted for **3**, which also involves the homoconjugated CMA cation. According to the above findings, it can be inferred that the interplay between attractive and repulsive effects due to the presence of molecules water results in the enhancement of the cohesive forces within **1** and **2**; however this effect does not seem to be the main factor determining the stability of CMA-based crystals investigated here.

The Hirshfeld surfaces

The Hirshfeld molecular surfaces divide the crystal into the regions, where the electron distribution of a sum of spherical atoms for the molecule dominates the corresponding sum over the crystal.[53,54] Thus, they reflect the directions and strength of intermolecular interactions within the crystal, mapped with different properties: the distance from the Hirshfeld surface to the nearest nucleus outside the surface (d_e), the corresponding distance to the nearest nucleus inside the surface (d_i) and a normalized contact distance (d_{norm}), shape index and curvedness (Figs 5 and S9†). The 2D plots of d_i *vs* d_e map the quantitative contribution and relative strength (color coded) of different intermolecular interactions, occurring within the crystal structures (Figs S10† and S11†).

The analysis of the Hirshfeld surfaces mapped by the d_{norm} property verified the presence of both hydrogen bonds and π–π interactions listed by the PLATON programme (Fig. 5, Tables S6†–S12†). For the molecular systems investigated (**1**–**3**) the π–π interactions are represented by relatively large flat areas in the curvedness surfaces (Fig. S9†). For **1** strong O–H···O hydrogen bond between O16 and O1W is marked on the d_{norm} surface as the red region, also present in the d_e and d_i surfaces (Figs 5 and S9†). In the case of compounds **2** and **3** weak hydrogen bonds type C–H···O and C–H···Cl are marked as pale red areas. The large red regions marked on the maps reflect short distances between O atoms, external and internal to the surface (d_e and d_i, respectively), as well as the presence

of mutual H atoms. All above mentioned interactions are presented in the two-dimensional fingerprint plots (d_e/d_i) (Figs S10† and S11†). The majority of the surface arises from the contribution of H···H interactions (from ca. 29% for **3** up to ca. 44% for **2**) (Figs 6, S10† and S11†) – which is characteristic for molecular crystals.[54] For **1** the O16–H16···O1W hydrogen bond between the acridinium cation and water molecule is represented by a single long spike (d_i between 0.6 and 1.2) in the O···H and H···O fingerprint plots (Figs S10† and S11†). For **2** and **3** such spikes do not occur; however smaller spikes (d_i values in the range of 1.1–1.6), indicating the presence of C–H···O hydrogen bonds among water molecules and CMA moieties or among CMA moieties themselves, are observed. Calculations for all compounds, performed with the assistance of the PLATON programme, disclose no signs of the existence of C–H···π interactions, which is further confirmed by the lack of characteristic wing motifs in the appropriate C···H and H···C fingerprint plots (Fig. S11). The acridinium acid moieties are involved in π–π type contacts, which is illustrated by the presence of green areas of the C···C contributions to the Hirshfeld surface (Fig. S11).

The relatively high share of the Cl···H and H···Cl contacts for **1** (4.5%) suggests the presence of a C–H···Cl interaction between the acridinium moiety and the chloride ion; however such an interaction was not found by the PLATON programme. In the case of compound **2** presence of the above-mentioned interactions is confirmed by both PLATON and the Hirshfeld surface (Cl···H and H···Cl fingerprint plot, Fig. S11). Relatively high contribution of H···F and F···H interactions (9.8%), disclosed for **3**, presumably results from the occurrence of disordered anionic fragment ($CF_3OSO_2^-$), in which the oxygen atoms may exchange with the fluorine ones.

Spectroscopic features

^{1}H and ^{13}C NMR spectra recorded for compounds **1**, **2** and **3** disclose a similar pattern, observed for previously investigated symmetric ACA derivatives (Figs S2†, S3†).[55]

The most deshielded protons, located in the spatial proximity of the nitrogen or oxygen atoms (H1/H8 and H4/H5, respectively (Fig. 1, Scheme S2†)), are manifested by the signals appearing in the form of two clear doublets. The remaining aromatic protons of the acridine ring system appear as the two distinct triplet systems – these are, in order of the increasing shielding, H3/H6 and H2/H7, respectively (Table S1A†).

In general, results of ^{1}H NMR experiments performed in various liquid phases (deuterium oxide, acetonitrile-d_3, methanol-d_4 and dimethylsulphoxide-d_6), do not suggest the existence of more than one form of the cations involved in **1**–**3** – or their mutual interconversion is too fast in comparison to the experiment time scale. Such a statement can be strictly drawn from the spectra, presenting only clear and well-shaped signals of all protons involved in the systems investigated as well as no changes in their intensity or shape upon lowering the temperature (in CD_3OD) (Figs S2B† and S2C†). This observation differentiates the behaviour of the compounds investigated in liquid environment from their behaviour in the crystalline solid or in the gas phase (discussed below), where

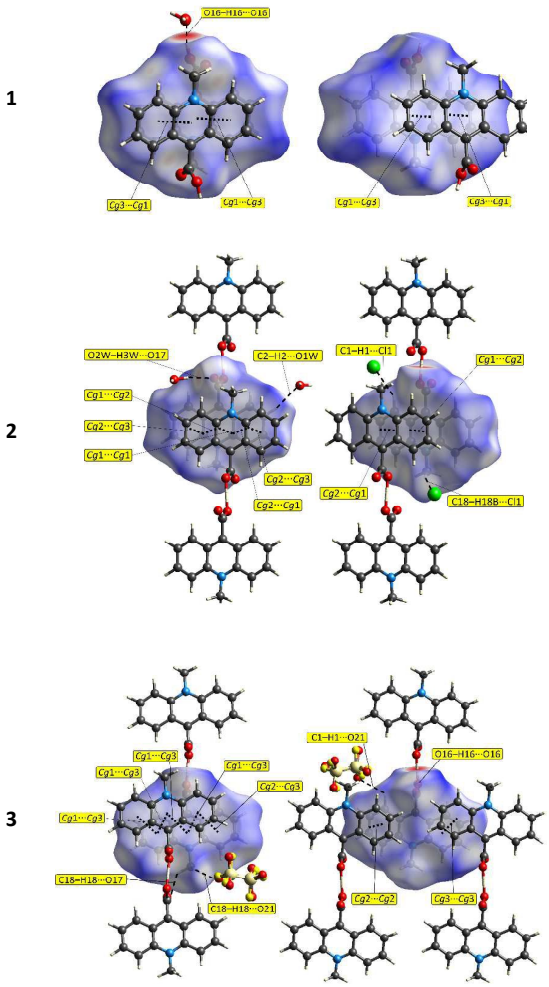

Fig. 5 The Hirshfeld surface (front (left) and reverse (right) views) of the 9-carboxy-10-methylacridinium moieties reflecting the normalized contact distance (d_{norm}) with selected interactions.

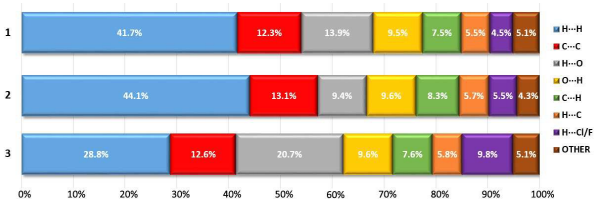

Fig. 6 Main contributions to the Hirshfeld surfaces from specific pairs of atom-types for 9-carboxy-10-methylacridinium moieties involved in compounds **1**-**3**. Contributions mentioned as others are for all compounds: C···O, O···C, C···N, N···C, H···N, N···H, O···O, O···N, N···O; in addition for **1**: C···Cl and for **3**: N···F.

various forms of these molecular systems are observed. Similar conclusions can be drawn from ^{13}C NMR spectra, recorded for **1–3** in deuterium oxide and dimethylsulphoxide-d6 (Table S1B†, Fig. S3†). The latter ones resemble the spectra of this type obtained for other quaternary derivatives of acridine-9-carboxylic acid investigated by us.[55]

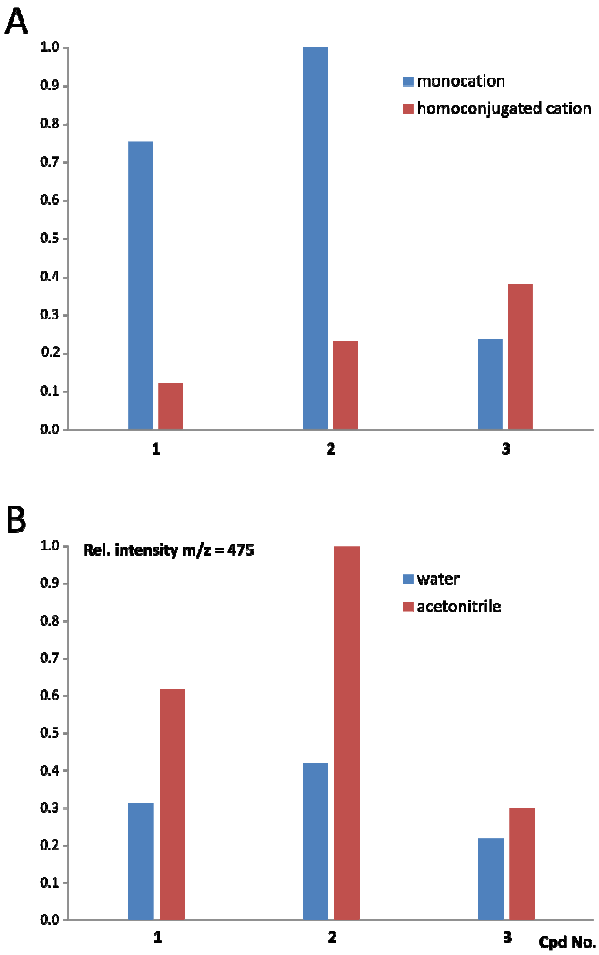

Fig. 7 The cations involved in compounds **1**, **2** and **3** in the gas phase found in the MALDI-TOF mass spectra. (**A**) The relative intensities (normalized) of the signals of monocationic form (m/z = 238) and homoconjugated cationic form (as a sum of signals of m/z = 475, 497 and 513). (**B**) The relative intensities (normalized) of the signals derived from homoconjugated cationic forms (m/z = 475) in the presence of various solvents used for sample preparation.

The MALDI-TOF mass spectra recorded for **1**–**3** (Table S2†, Fig. S12†) indicate that, in the case of **1** and **2**, the monocationic form prevails over the homoconjugated form of CMA in the gas phase; however, for **3** the situation seems to be reversed (Fig. 7, Table S3†). Contents of the homoconjugated cations in the gas phase increases in the order of **1**, **2** and **3**, which reveals that cations of **1** (appearing in a crystalline solid phase in the monomeric form) and **3** (appearing in a crystalline solid phase exclusively in the homocojugated form) are characterized by the lowest and the highest amount of the former one in the gaseous phase, respectively. This allows to conclude that the molecular systems under investigation are characterized by the occurrence of equilibrium between the two above-mentioned forms and their population in the gas phase depends on the chemical environment and experimental conditions. The latter statement is supported by the comparison of the population of monocationic *vs* homoconjugated forms, characterizing cations **1**–**3** when protic medium (water) *vs* non-protic one (acetonitrile) is used for preparation of samples (Fig. 7,Table S3†). The experiments reveal, that amount of the

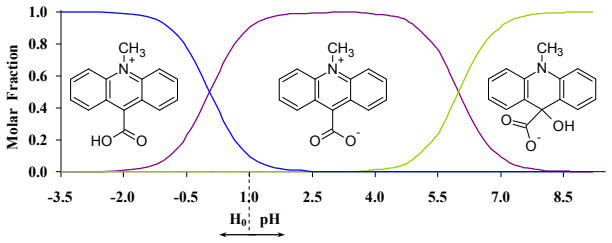

Fig. 8 Mole fractions of the forms of **1** *versus* pH/H_0 estimated basing on the experimentally determined first ionization constant (pK_a(1) = 0.05) and the theoretically predicted second ionization constant (pK_a(2) = 6.0). See also Table S4† and Fig. S13†.

monocationic form of CMA decreases in an anhydrous conditions if compared to aqueous ones, indicating occurrence of equilibrium between both forms in gaseous phase. A high-resolution UPLC/ESI-QTOF mass spectra were additionally recorded for **1** and **3** (see Figs 13† and 14† and text below).

To understand the origin of the unique behaviour of CMA in solid phase, one should take into account the composition of solutions used for crystal growth. As CMA contains groups, that are able to participate in protolytic transformations, its actual form in aqueous solutions depends on the acidity of environment (pH/H_0). The protolytic forms of CMA are characterized by different spectral properties, which allowed us to determine the ranges of pH/H_0 in which these species are thermodynamically stable, performing spectrophotometric UV-Vis acid-base titration (Table S4†, Fig. S15†). In solutions of high acidity (H_0 < –2.0) CMA exists in the mono-protonated form – (monocation, Fig. 8). In solutions of lower acidity (–2.0 < H_0/pH < 2.0) the monocationic form coexists with the zwitterionic one (Fig. 8), the pK_a value of this protolytic equilibrium is 0.05 ± 0.01 (Table S4†). The pK_a values, calculated at various wavelengths in the UV-Vis spectra, change slightly in a systematic manner, which likely arises from the changes in ionic strength of the titrated solution.

The equilibrium between monocationic and zwitterionic forms, characterized by pK_a value of 1.72, was assessed in the past in the aqueous solutions containing 3-carboxy-1-methylpyridinium cation, structurally related to CMA.[56] Zwitterionic form of CMA is thermodynamically stable in solutions of low acidity and it transforms to a pseudo-base form in neutral and basic environments (Fig. 8) – similarly to other 10-methylacridinium derivatives.[57] Since the crystals of **1**–**3** were grown in the protic solutions of various acidity, the co-existence of monocationic and zwitterionic forms in such media is of special interest for understanding the origin of formation of CMA-based homoconjugated cations, discussed below.

Computational predictions

Structural considerations

Calculations carried out at the DFT level of theory for the reagents in gaseous phase enabled to propose the structures of monomeric (**1a**–**1c**) and homocojugated (**2a**–**2e**, **3a**–**3c**) forms of CMA, that might be involved in **1**–**3** (Fig. S16†). Other

Table 2 Structural features and thermodynamic data of conformers of the compounds **1**–**3**.

Entity	Method[a]	Geometry of the O–H···O hydrogen bond				Angle (°)				ΔH_{rel}	ΔG_{rel}	μ[c]
		O–H	H···O	O···O	<(OHO)	A[b]	B[b]	C[b]	D[b]			
1a	X-ray							89.6				
	DFT							51.5				17.6
1b	DFT							58.5		292.2[d]	291.8[d]	11.0
1c	DFT							57.6		292.5[d]	288.4[d]	11.5
2a	X-ray	1.220	1.220	2.435	180	0.0	0.0	84.8	84.8			
	DFT	1.068	1.419	2.486	176	3.8	61.4	64.5/69.2	67.3/60.9	27.4[e]	29.9[e]	11.5
2b	DFT	1.047	1.472	2.513	172	49.2	74.8	66.6/72.7	38.8/38.5			29.1
2c	DFT	1.056	1.448	2.498	172	55.6	75.2	71.0/73.3	40.3/38.5	2.6[f]	–0.9[f]	28.6
2d	DFT	1.038	1.517	2.492	154	60.3	72.6	68.8/75.3	44.4/82.2			6.9
2e	DFT	1.117	1.320	2.434	174	47.3	77.6	69.2/70.7	38.5/34.4			14.9
3a	X-ray	1.220	1.220	2.449	180	0.0	0.0	88.2	88.2			
	DFT	1.042	1.509	2.485	153	51.5	72.3	78.8/79.3	50.3/82.5			7.2
3b	DFT	1.052	1.456	2.502	172	52.3	73.4	74.0/69.7	38.0/42.7	13.5[g]	5.5[g]	37.3
3c	DFT	1.158	1.261	2.416	174	44.1	76.7	68.2/68.4	39.2/38.1			4.0

[a] DFT – the DFT(B3LYP)/6-31G** level of theory;
[b] A, between the mean plane of the first acridine nucleus (C1–C14, N10) and the second acridine nucleus (C1A–C14A, N10A); B, between the mean planes delineated by C15, O16, O17 and C15A, O16A, O17A; C, between the mean plane of the first acridine nucleus (C1–C14, N10 or C1A–C14A, N10A) and the mean plane of the carbonyl group of the same acridine nucleus (C15, O16, O17 or C15A, O16A, O17A); D, between the mean plane of the first acridine nucleus (C1–C14, N10 or C1A–C14A, N10A) and the mean plane of the carbonyl group of the second acridine nucleus (C15A, O16A, O17A or C15, O16, O17).
[c] μ represents the dipole moment of the compounds (indicated in Fig. S14†), in *D*;
[d] ΔH_{rel} and ΔG_{rel} represent the enthalpy and the Gibbs' free energy of a given conformers (indicated in Fig. S14†) relative to the enthalpy and the Gibbs' free energy of **1a** form; ΔH_{rel} and ΔG_{rel} values, in kJ mol^{-1};
[e] ΔH_{rel} and ΔG_{rel} represent the enthalpy and the Gibbs' free energy of a given conformer (indicated in Fig. S14†) relative to the enthalpy and the Gibbs' free energy of **2b** form; ΔH_{rel} and ΔG_{rel} values, in kJ mol^{-1};
[f] ΔH_{rel} and ΔG_{rel} represent the enthalpy and the Gibbs' free energy of a given conformer (indicated in Fig. S14†) relative to the enthalpy and the Gibbs' free energy of **2d** form; ΔH_{rel} and ΔG_{rel} values, in kJ mol^{-1};
[g] ΔH_{rel} and ΔG_{rel} represent the enthalpy and the Gibbs' free energy of a given conformer (indicated in Fig. S14†) relative to the enthalpy and the Gibbs' free energy of **3a** form; ΔH_{rel} and ΔG_{rel} values, in kJ mol^{-1}.

forms, including classical dimeric ones (containing two O–H···O hydrogen bonds) were also considered, but are not included in further analysis as high energetic (thermodynamically unstable). The structural and thermodynamic data, summarized in Tables 2 and S16†, concerns the possible vapour phase complexes, that may be formed with the participation of CMA, chloride or triflate anions and water molecules. Optimization of the monomeric structures leads to the thermodynamically most stable form **1a** (Table 2). The enthalpy and Gibbs free energy differences ($\Delta_{rel}H$ and $\Delta_{rel}G$, respectively) between the latter structure and the two less stable monomeric forms (**1b**, **1c**) are substantial, assuming values of 292.2 and 292.5 ($\Delta_{rel}H$) and 291.8 and 288.4 ($\Delta_{rel}G$) kJ mol^{-1}, respectively.

The computational studies, carried out on the homoconjugated forms of CMA, enabled to propose the three types of structure: linear (**2a**, **2c** and **3b**), bent (**2b**, **2d** and **3a**) and flat ones (**2e** and **3c**) (Fig. S16†). Linear and bent forms refer to the hydrogen bond (O–H···O) geometry; flat form refers to the anion···cation–H–cation···anion geometry. As regards to the homoconjugates type **2** and **3**, the bent structures, characterized by small value of the dipole moment, are thermodynamically preferred in the gas phase (Table S14). According to that, in both types of salts – that is, the one comprising Cl^- and $CF_3SO_3^-$ counter anions (**2d** and **3a**, respectively, Fig. S16†) – the more stable bent structures are also characterized by lower values of the dipole moment (Table 2). However, in the case of complexes composed of the homoconjugated cation, chloride anion and two molecules of water (structures **2a** and **2b**, Fig. S16†), the dipole moment assumes substantially higher values (11.5 and 29.1, respectively) – although energetically favourable arrangement is also bent (**2b**). The latter likely results from the replacement of the Cl^- and H_2O moieties towards one of the N atoms of the acridine ring system (in the case of **2b**), while in the linear complex (**2a**), the Cl^- and H_2O remain in a central position – i.e. in the vicinity of the H-bond, binding both CMA moieties. In the case of negatively charged molecular complexes containing two anions (**2e** and **3c**, Fig. S16†), the more stable structure is flat, with the anions shifted towards the nitrogen atoms (N10 and N10A). In the case of linear homoconjugated forms (**2a**, **2c**, **3b**, Fig. S16†), the O···H–O hydrogen bond is slightly shorter as compared to its length, specifies for the bent arrangements (**2b**, **2d**, **3a**, Fig. S16†) (although the enthalpy and Gibbs free energies of such complexes are higher (Table 2 and S16†). Geometry of hydrogen bonding in the homoconjugated cations resembles the one determined in the case of the crystalline phases (**2** and **3**). However, the H-atom involved in it is insignificantly shifted towards one of the oxygen atoms, resulting in the formation of slightly unsymmetrical hydrogen bonding (Table 2 and Fig. S16†). As it was discussed above, stability of the optimized complexes is controlled mainly by the electrostatic interactions, occurring among the positively charged N atoms and $CF_3SO_3^-$ or Cl^- anions. In the bent complexes (**2d**, **3a**, Fig. S16†) the $N^+\cdots A^-$ distances are relatively short, attaining the values of 4.045/7.808 Å for $CF_3SO_3^-$ and 3.686/7.680 Å for Cl^-, respectively, while in the case of the linear ones (**2c**, **3b**, Fig. S16†) – shorter (comparable to the above ones) and longer $N^+\cdots A^-$ distances were predicted (5.228/15.878 Å for $CF_3SO_3^-$ and 4.319/14.121 Å for Cl^-). The situation is different in the case of complexes containing molecules of water – in the flat structure **2a** the distances are comparable (7.539 and 7.360 Å for $CF_3SO_3^-$ and Cl^-, respectively), while in the bent complex **2b** these distances are similar to those found for the linear ones, attaining values of 4.265 and 14.403 Å, respectively. The latter effect is presumably a consequence of distinct shift of the chloride anion together with water molecules towards one of the nitrogen atoms (N10 or N10A), followed by bending of the whole molecular arrangement.

Generally, DFT calculations indicate, that incorporation of water molecules into the investigated molecular complexes is manifested in the thermodynamic stabilization of resultant

structures; a linear complexes are less stable than the bent ones by about 27.2 and 29.7 kJ mol^{-1} (respective differences in enthalpy and Gibbs free energy). In the case of chloride complex this effect is not distinctly pronounced – the linear architecture is less stable than the bent one by 2.5 kJ mol^{-1} (enthalpy). In the linear complex **2a** the N10···O(w) distances are comparable and distributed quite symmetrically (the values of 5.769, 6.657, 6.771 and 10.661 Å), while in the bent complex **2b** a distinct shift of water molecules towards the acridinium N atoms is observed (the values of 4.149, 14.917, 4.653 and 15.934 Å).

The vapour phase-optimized structure of the monomeric form, associated with two molecules of water and the chloride counter ion (**1a**), closely resembles the architecture, characterizing crystalline solid phase (that is **1**, built of CMA monocations). As it was mentioned above, the latter form is also energetically favoured among considered monocationic forms – as the other ones are less stable by about 290 kJ mol^{-1} (Table S14†, Fig. S16†).

Pathways of formation of the homoconjugated cations

Calculations of basic thermodynamic data (enthalpies and Gibbs free energies) carried out at the DFT level of theory for the reagents in gaseous and liquid phases (water and ethanol) enabled to propose the pathway of formation of the homoconjugated CMA-based forms, involved in compounds **2** and **3**. The formation of homoconjugated cation and the zwitterionic form of CMA (CMA/z), is energetically more favourable than the formation of the dimer, consisting of two CMA cations (data not shown). The formation of the homoconjucated form is thermodynamically probable, as the enthalpy ($\Delta_{r,298}H^o$) and Gibbs free energy ($\Delta_{r,298}G^o$) attain the values of −178.6 and −132.1 kJ mol^{-1}, respectively (Table 3). In the case of dimeric form, the calculated $\Delta_{r,298}H^o$ and $\Delta_{r,298}G^o$ energies are higher, expressing values of 64.4 and 112.0 kJ mol^{-1}, respectively. Taking into account transformation pathways leading to the formation of homoconjugated forms involved in **2** and **3**, as well as the above-discussed findings (*Spectroscopic features* section), we considered the possible processes, which may explain the experimental observations. Scheme 1 presents probable transformation pathways, involving various forms of CMA in protic environment (water/ethanol). According to that, step I denotes the equilibrium, that may occur between zwitterionic and the 'pseudobase'[8] form of CMA; step II – the formation of the homocojugated cation from the above two forms; step III – the equilibrium between zwitterionic and monocationic form of CMA with the participation of hydronium ion and step IV – the formation of the homoconjugated cation from the zwitterionic and monocationic forms of CMA.

Scheme 1 Probable pathways of formation of homoconjugated bis(9-carboxy-10-methylacridinium) cations proposed at the level of DFT method.

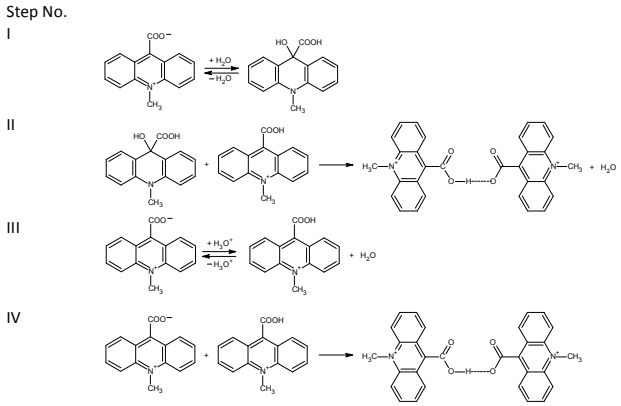

The theoretically predicted thermodynamic data for possible transformation pathways summarized in Table 3, indicate that the above described steps are probable only in the gaseous phase. In liquid phase (H_2O or CH_3CH_2OH), step I seems to be thermodynamically unfavourable (positive value of Gibbs free energy). Predicted thermodynamic data suggest, that formation of the homoconjugated cations presumably take place according to the transformation steps denoted as III and IV (Scheme 1). The latter two pathways underline our above-stated findings, indicating, that the formation of homoconjugated cations of CMA occurs in solid crystalline and gaseous phases.

Table 3. Thermodynamic data (in kJ mol^{-1}) for consecutive steps of formation of hydrogen-bis(9-carboxy-10-methyacridinium) cation[a].

Step[b]	Phase	Method	Δ*H*	Δ*G*
I	gaseous	DFT/6-31G**	−78.0	−27.7
	liquid	DFT (PCM-H_2O)/6-31G**		34.5
		DFT (PCM-CH_3CH_2OH)/6-31G**		31.9
II	gaseous	DFT/6-31G**	−100.6	−104.4
	liquid	DFT (PCM-H_2O)/6-31G**		−72.6
		DFT (PCM-CH_3CH_2OH)/6-31G**		−73.3
III	gaseous	DFT/6-31G**	−358.7	−353.0
	liquid	DFT (PCM-H_2O)/6-31G**		−144.0
		DFT (PCM-CH_3CH_2OH)/6-31G**		−150.7
IV	gaseous	DFT/6-31G**	−178.6	−132.1
	liquid	DFT (PCM-H_2O)/6-31G**		−38.0
		DFT (PCM-CH_3CH_2OH)/6-31G**		−41.4

[a] Δ*H* and Δ*G* denote enthalpy and Gibbs free energy of the reaction (step), respectively.
[b] For possible pathways of formation of the title cation see Scheme 1.

Conclusions

Newly synthesized quaternary acridinium salts of cognitive and practical interest, namely 9-carboxy-10-methylacridinium chloride (CMACl) and 9-carboxy-10-methylacridinium trifluoromethansulfonate (CMATfO), were synthesized and subjected to through physicochemical – experimental and theoretical – investigations. Various crystalline forms of the above CMA-based salts, encoded as compounds **1**, **2** and **3** were investigated with the aim of single crystal X-ray diffraction analysis, crystal lattice energy calculations, determination of Hirshfeld surfaces, MALDI-TOF mass spectrometry, ^{1}H and ^{13}C NMR and UV-Vis spectroscopy, as well as quantum chemistry method, basing on the Density Functional Theory (DFT). Geometry, spatial architecture of the entities ordered in the crystalline forms, intermolecular interactions, occurring in the solid and gaseous phases as well

as the thermodynamics and their origin are also elucidated in the work.

Compounds **1**–**3**, presented in Fig. 1 are, in general, similar in terms of molecular geometry to other acridinium salts investigated by us, being characterized by planar acridine ring system and a carboxyl group twisted at ca. right angle relative to the acridine nucleus. Chlorides **1** and **2** crystallize in the monoclinic space group, while the triflate **3** crystalizes in the triclinic space group. As it was detected using PLATON programme, predominant role in the crystal packings of **1**–**3** play hydrogen bonds of various strength (O–H···O, C–H···O) or halogen (X)-containing specific intermolecular interactions, such as O–H···X and C–H···X. Parallely oriented aromatic layers in the crystals are stabilized by the network of π–π contacts and non-specific dispersive interactions, that occur between aromatic rings of adjacent acridinium moieties – resulting in the formation of characteristic multi-layered frameworks. In homoconjugated forms **2** and **3**, symmetric O–H···O hydrogen bond occurs, in which the H-atom is located directly in the inversion centre. The observed features of the crystalline networks are responsible for major differences in conformation, H-bond patterns and calculated lattice energies, characterizing crystalline solid phases of the investigated systems. The reason of the observed physicochemical features of the crystalline solids presumably lies in the presence or absence of water molecules and fluorine atoms, involved in a complex network of short-range interactions revealed in **1**, **2** and **3**.

Computational methods, implemented in GULP program, used for evaluation of the crystal lattice energies, provided the thermodynamic characteristics of the systems. Theoretically predicted lattice energies (E_L, Table 1) reveal that the lattices characterizing **1**–**3** significantly differ in terms of their stability, namely compound **3** appears as the one forming the most stable crystals and the compound **2** the least stable. In **1** the major attractive force occurring within the crystal lattice was found to be the electrostatic one (E_{el}). Here, dispersive E_d term is almost entirely suppressed by the repulsion E_r term. In turn, dispersion dominates in E_L assessed for crystals of **2**, whereas in crystals of **3**, E_{el} and E_d contributions to E_L express similar magnitude. The influence on the thermodynamic stability of crystals exerted by water molecules within lattices of **1** and **2** was also elucidated. In general, the presence of H_2O within the crystal structures is manifested by the increase in total cohesive forces by more than 100 kJ mol^{-1}; however, this effect, when compared to the large E_L values, seems not to be of fundamental importance for the stabilization of crystal lattices of **1** and **2**.

The analysis of Hirshfeld surfaces, designated for **1**–**3** verified the presence of hydrogen bonds and π–π contacts, commonly occurring within the investigated molecular systems (Figs 5 and 6). The red or pale red areas on the surfaces correspond to a various types of hydrogen bonds and indicate shorter or longer mutual distances of the selected atoms. The O–H···O and C–H···O interactions are represented by longer or shorter single spikes on the fingerprint plots – accordingly to relative energy of the above interactions, while π–π contacts are represented by large flat regions characterizing the Hirshfeld surfaces.

Spectroscopic methods, such as MALDI-TOF MS, ^{1}H and ^{13}C NMR and UV-Vis allowed us to get further insight into the structures of **1–3** in gaseous and liquid phases. The mass spectra revealed, that in the gas phase the equilibrium occurs between the monocationic and homoconjugated forms of CMA, wherein their population depends on the experiment condition; hydrated cations, involved in crystals of **1** and **2** were not observed in the MALDI-TOF experiments. ^{1}H and ^{13}C NMR spectra, obtained for **1**–**3** in various liquid phases (D_2O, DMSO-d_6, CD_3OD, CD_3CN) and at different temperatures (300 and 233 K, CD_3OD), disclosed that forms of CMA are not distinguishable by this method, or one form is present under the conditions of experiments. Spectrophotometric acid-base titration of **1** (built of the monocationic form of CMA), performed in aqueous environment, revealed, that CMA may exist in the monocationic or zwitterionic forms under the conditions of crystal growth, which, gives rise to the formation of the homoconjugated cations found in crystals of **2** and **3**.

According to quantum chemistry calculations (DFT level of theory), conducted for **1**–**3** in the gas phase, the structural data obtained theoretically is comparable to the experimental findings (single crystal X-ray crystallography) (Table 2, 3 and S13†). Thermodynamic stability of the homoconjugated cations relates to O–H···O hydrogen bond length as well as an attractive electrostatic interactions, occurring among the oppositely charged group of atoms (the N atoms experiencing deficit of electron density and Cl^- or $CF_3OSO_2^-$ anions). The above-mentioned features of investigated molecular systems are also reflected in their various dipole moments. Basing on the DFT approach, we proposed a possible pathways of formation of CMA-based forms studied here. Calculated thermodynamic data emphasize an experimental findings, revealing that the formation of the homoconjugated forms of CMA is likely to occur in crystalline solid and liquid phases.

Acknowledgements

Financial support is acknowledged from the State Funds for Scientific Research through National Science Centre grants No. DEC-2012/05/B/ST5/01680 (contract No. UMO-2012/05/B/ST5/01680) and N N204 375 740 (contract No. 3757/B/H03/2011/40). Computer time was granted from Wroclaw Centre for Networking and Supercomputing (WCSS, Poland) under grants no. 196 and 215 and the Tri-City Academic Computer Centre in Gdansk (TASK, Poland). This research was also supported in part by PL-Grid Infrastructure. BZ acknowledges financial support from the European Social Fund within the project "The development program of the University of Gdansk in areas of Europe 2020 (UG 2020)". The authors would thank to M.Sc. Paweł Wityk for his valuable help in recording of UPLC/ESI-QTOF MS spectra.

References

1 K. Smith, J.-J. Yang, Z. Li, I. Weeks and J. S. Woodhead, *J. Photochem. Photobiol. A: Chem*., 2009, **203**, 72.
2 K. Krzymiński, A. D. Roshal, B. Zadykowicz, A. Białk-Bielińska and A. Sieradzan, *J. Phys. Chem. A*., 2010, **114**, 10550.
3 A. Roda and M. Guardigli, *Anal. Bioanal. Chem*., 2012, **402**, 69.
4 A. Natrajan and D. Sharpe, *Org. Biomol. Chem*., 2013, **11**, 1026.
5 J. Dey, J. L. Haynes III, I. M. Warner and A. K. Chandra, *J. Phys. Chem. A*., 1997, **101**, 2271.
6 K. Krzymiński, A. D. Roshal and A. Niziołek, *Spectrochim. Acta, Part A*., 2008, **70**, 394.
7 K. Krzymiński, P. Malecha, P. Storoniak, B. Zadykowicz and J. Błażejowski, *J. Therm. Anal. Cal*., 2010, **100**, 207.
8 M. W. Cass, E. Rapaport and E. H. White, *J. Am. Chem. Soc.*, 1971, **94**, 3168.
9 L. J. Kricka, *Anal. Chim. Acta*., 2003, **500**, 279.
10 Y. Kitamura, T. Iwasaki, M. Saito, M. Mifune, Y. Saito, K. Sato, C. Yomota and K. Tanamoto, *J. Food Hyg. Soc. Japan*, 2006, **47**, 232.
11 Z. Dega-Szafran, A. Kartusiak and M. Szafran, *J. Mol. Struct*., 2006, **785**, 160.
12 J. Rak, P. Skurski and J. Błażejowski, *J. Org. Chem.*, 1999, **64**, 3002.
13 K. Krzymiński, A. Ożóg, P. Malecha, A. D. Roshal, A. Wróblewska, B. Zadykowicz and J. Błażejowski, *J. Org. Chem*., 2011, **76**, 1072.
14 CrysAlis CCD and CrysAlis RED, Oxford Diffraction Ltd., Yarnton, England, 2008.
15 G. M. Sheldrick, *Acta Cryst. Sect. A*., 2008, **64**, 112.
16 A. L. Spek, *Acta Cryst. Sect. D*., 2009, **65**, 148.
17 C. K. Johnson, ORTEP II, Report ORNL-5138, Oak Ridge National Laboratory, Oak Ridge, TN, USA, 1976.
18 S. Motherwell and S. Clegg, PLUTO-78, Program for Drawing and Molecular Structure, University of Cambridge, UK, 1978.
19 C. F. Macrae, I. J. Bruno, J. A. Chisholm, P. R. Edgington, P. McCabe, E. Pidcock, L. Rodriguez-Monge, R. Taylor, J. Van de Streek and P. A. Wood, *J. Appl. Cryst.*, 2008, **41**, 466.
20 (a) J. D. Gale, *J. C. S. Faraday Transactions*, 1997, **93**, 629; (b) J. D. Gale and A. L. Rohl, *Mol. Simul.*, 2003, **29**, 291.
21 J. K. Labanowski and J. K. Andzelm (Eds), *Density functional methods in chemistry*, New York, Springer, 1991.
22 (a) U. C. Singh and P. A. Kollman, *J. Comp. Chem.*, 1984, **5**, 129; (b) B. H. Besler, K. M. Merz Jr. and P. A. Kollman, *J. Comp. Chem.*, 1990, **11**, 431.
23 Y. Zhao and D. G. Truhlar, *Theor. Chem. Acc.*, 2008, **120**, 215.
24 (a) R. Ditchfield, W. J. Hehre and J. A. Pople, *J. Chem. Phys.*, 1971, **54**, 724; (b) W. J. Hehre, R. Ditchfield and J. A. Pople, *J. Chem. Phys.*, 1972, **56**, 2257.
25 M. J. Frisch, G. W. Trucks, H. B. Schlegel, G. E. Scuseria, M. A. Robb, J. R. Cheeseman, G. Scalmani, V. Barone, B. Mennucci, G. A. Petersson, H. Nakatsuji, M. Caricato, X. Li, H. P. Hratchian, A. F. Izmaylov, J. Bloino, G. Zheng, J. L. Sonnenberg, M. Hada, M. Ehara, K. Toyota, R. Fukuda, J. Hasegawa, M. Ishida, T. Nakajima, Y. Honda, O. Kitao, H. Nakai, T. Vreven, J. A. Montgomery. Jr., J. E. Peralta, F. Ogliaro, M. Bearpark, J. J. Heyd, E. Brothers, K. N. Kudin, V. N. Staroverov, T. Keith, R. Kobayashi, J. Normand, K. Raghavachari, A. Rendell, J. C. Burant, S. S. Iyengar, J. Tomasi, M. Cossi, N. Rega, J. M. Millam, M. Klene, J. E. Knox, J. B. Cross, V. Bakken, C. Adamo, J. Jaramillo, R. Gomperts, R. E. Stratmann, O. Yazyev, A. J. Austin, R. Cammi, C. Pomelli, J. W. Ochterski, R. L. Martin, K. Morokuma, V. G. Zakrzewski, G. A. Voth, P. Salvador, J. J. Dannenberg, S. Dapprich, A. D. Daniels, O. Farkas, J. B. Foresman, J. V. Ortiz, J. Cioslowski and D. J. Fox, Gaussian 09, Revision D.01,Gaussian. Inc., Wallingford CT, 2013.
26 S. L. Mayo, B. D. Olafson and W. A. Goddard, *J. Phys. Chem.*, 1990, **94**, 8897.
27 G. Filippini and A. Gavezzotti, *Acta Cryst. Sect. B*, 1993, **49**, 868.
28 B. Zadykowicz, K. Krzymiński, P. Storoniak and J. Błażejowski, *J Therm. Anal. Cal.*, 2010, **101**, 429.
29 S. K. Wolff, D. J. Grimwood, J. J. McKinnon, M. J. Turner, D. Jayatilaka and M. A. Spackman, CrystalExplorer (Version 3.1), University of Western Australia, 2012.
30 A. Williams, S. Bakulin and S. Golotvin, NMR Prediction Software, Advanced Chemistry Development, Toronto, 2001, http://www.acdlabs.com.
31 K. Pigoń and Z. Ruziewicz, *Physical Chemistry, Vol. 1: Phenomenological basics*, PWN, Warsaw, 2005, p. 334.
32 R. A. Cox and K. Yates, *Can. J. Chem.*, 1981, **59**, 2116.
33 A. O. Doroshenko, Spectral Data Lab software, Kharkiv, 1999.
34 J. Reijenga, A. van Hoof, A. van Loon and B. Teunissen, *Anal. Chem. Ins*., 2013, **8**, 53.
35 (a) Ü. Haldna, *Prog. Phys. Org. Chem.*, 1990, **18**, 65; (b) Ü. Haldna and A. Murshak, *Comput. Chem.*, 1988, **8**, 201.
36 H. B. Schlegel (Ed.), *Modern Electronic Structure Theory: Geometry Optimization on Potential Energy Surfaces*, World Scientific Publishing, Singapore, 1994.
37 (a) P. C. Hariharan and J. A. Pople, *Theor. Chim. Acta*, 1973, **28**, 213, (b) W. J. Hehre, L. Radom, P. v. R. Schleyer and J. A. Pople (Eds), *Ab Initio Molecular Orbital Theory*, Wiley, New York, 1986.
38 (a) A. D. Becke, *Phys. Rev. A*, 1988, **38**, 3098, (b) A. D. Becke, *J. Chem. Phys*., 1993, **98**, 1372.
39 C. Lee, W. Yang and R. G. Parr, *Phys. Rev. B*, 1988, **37**, 785.
40 M. J. S. Dewar and G. P. Ford, *J. Am. Chem. Soc.*, 1977, **99**, 7822.
41 ChemCraft, Version 1.6 (build 350), http://www.chemcraftprog.org.
42 D. Trzybiński, K. Krzymiński, A. Sikorski, P. Malecha and J. Błażejowski, *Acta Cryst Sect. E*., 2010, **66**, o826.
43 D. Trzybiński, K. Krzymiński, A. Sikorski and J. Błażejowski, *Acta Cryst Sect. E*., 2010, **66**, o906.
44 D. Trzybiński, K. Krzymiński, A. Sikorski and J. Błażejowski, *Acta Cryst Sect. E*., 2010, **66**, o1313.
45 D. Trzybiński, K. Krzymiński and J. Błażejowski, *Acta Cryst Sect. E*., 2010, **66**, o2773.
46 M. Mirzaei, H. Eshtiagh-Hosseini, M. Bazargan, F. Mehrzad, M. Shahbazi, J.T. Mague, A. Bauzá and A. Frontera, *Inorg. Chim. Acta*, 2015, **438**, 135.
47 H. Eshtiagh-Hosseini, M. Mirzaei, S. Zarghami, A. Bauzá, A. Frontera, J.T. Mague, M. Habibi and M. Shamsipur, *CrystEngComm*, 2014, **16**, 1359.
48 M. Mirzaei, H. Eshtiagh-Hosseini, Z. Karrabi, K. Molčanov, E. Eydizadeh, J.T. Mague, A. Bauzá and A. Frontera, *CrystEngComm*, 2014, **16**, 5352.
49 G. E. Bacon and N. A. Curry, *Acta Cryst.*, 1960, **13**, 717.
50 L. Manojlović and J. C. Speakman, *Acta Cryst. Sect. B*., 1968, **24**, 323.
51 J. C. Speakman, *Struct. Bond.*, 1972, **12**, 141.
52 N. K. Kalsbeek and S. Larsen, *Acta Cryst. Sect C*., 1991, **47**, 1005.
53 J. J. McKinnon, M. A. Spackman and A. S. Mitchell, *Acta Cryst. Sect. B*, 2004, **60**, 627.
54 P. Panini, T. P. Mohan, U. Gangwar, R. Sankolli and D. Chopara, *CrystEngComm*, 2013, **15**, 4549.
55 K. Krzymiński, P. Malecha, B. Zadykowicz, A. Wróblewska and J. Błażejowski, *Spectrochim. Acta., Part A*, 2011, **78**, 401.
56 M. L. Black, *J. Phys. Chem.*, 1955, **59**, 670.
57 J. W. Bunting, V. S. F. Chew, S. B. Abhyankar and Y. Goda, *Can. J. Chem.*, 1984, **62**, 351.

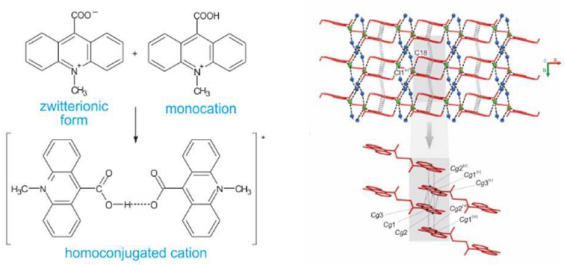

New crystalline compounds, containing monomeric and homoconjugated forms of 9-carboxy-10-methylacridinium cations were obtained and investigated. Through experimental and theoretical studies on their structural, spectroscopic and thermodynamic features are addressed in the article.